processes

MDPI

Article

The Activity and Stability of Promoted Cu/ZnO/Al_2O_3 Catalyst for CO_2 Hydrogenation to Methanol

Nor Hafizah Berahim [1,2,*], Noor Asmawati Mohd Zabidi [2], Raihan Mahirah Ramli [3] and Nur Amirah Suhaimi [2]

[1] Group Research & Technology, Carbon Capture, Utilization & Storage Department, PETRONAS Research Sdn. Bhd., Kajang 43000, Selangor, Malaysia
[2] Center of Contaminant Control and Utilization (CenCoU), Institute of Contaminant Management for Oil and Gas, Department of Fundamental and Applied Sciences, Universiti Teknologi PETRONAS, Seri Iskandar 32610, Perak, Malaysia
[3] Centre of Innovative Nanostructures & Nanodevices (COINN), Department of Chemical Engineering, Universiti Teknologi PETRONAS, Seri Iskandar 32610, Perak, Malaysia
* Correspondence: hafizah.berahimjusoh@petronas.com; Tel.: +60-3-8928-1183

Abstract: Cu/ZnO/Al_2O_3 catalyst with the addition of tri-promoters (Mn/Nb/Zr) was investigated with respect to their catalytic activity and stability in a prolonged reaction duration in methanol synthesis. Spent catalysts were characterized using N_2 adsorption-desorption, FESEM/EDX, TEM, N_2O chemisorption, and XPS for their physicochemical properties. The catalyst longevity study was evaluated at two days, seven days, and 14 days at 300 °C, 31.25 bar, 2160 mL/g.hr GHSV, and H_2:CO_2 at 10:1. The CO_2 conversion and methanol yield decreased by about 5.7% and 7.7%, respectively, when the reaction duration was prolonged to 14 days. A slight reduction in catalytic activity under prolonged reaction duration was found due to thermal degradation.

Keywords: Cu/ZnO/Al_2O_3 catalyst; methanol synthesis; stability; activity

Citation: Berahim, N.H.; Zabidi, N.A.M.; Ramli, R.M.; Suhaimi, N.A. The Activity and Stability of Promoted Cu/ZnO/Al_2O_3 Catalyst for CO_2 Hydrogenation to Methanol. *Processes* **2023**, *11*, 719. https://doi.org/10.3390/pr11030719

Academic Editors: Sara Liparoti and Qian Xu

Received: 26 November 2022
Revised: 8 February 2023
Accepted: 21 February 2023
Published: 28 February 2023

1. Introduction

Since Imperial Chemical Industries' (ICI) discovery of a low-temperature and low-pressure Cu/Zn/Al_2O_3 catalyst in 1966, the Cu/Zn/Al_2O_3 catalyst has been widely utilized in industrial methanol synthesis [1,2]. Commercially, methanol has been synthesized from syngas, which primarily comprises CO and H_2 with a trace quantity of CO_2 [3,4]. Methanol synthesis from CO_2 hydrogenation has recently received a lot of attention as one of the most promising CO_2 mitigation strategies. Several studies on the production of methanol from CO_2 hydrogenation have been reported [5–12]. The synthesis of methanol from CO_2 hydrogenation can be seen from two angles. CO_2 is transformed directly to methanol in Equation (1), but there is also an indirect pathway via the reverse water-gas shift (RWGS) in Equation (2) and CO hydrogenation in Equation (3).

$$CO_2 + 3H_2 \leftrightharpoons CH_3OH + H_2 \qquad \Delta H^\circ\ 298K = -49.5\ kJ/mol \quad (1)$$

$$CO_2 + H_2 \leftrightharpoons CO + H_2O \qquad \Delta H^\circ\ 298K = +41\ kJ/mol \quad (2)$$

$$CO + 2H_2 \leftrightharpoons CH_3OH \qquad \Delta H^\circ\ 298K = -90.5\ kJ/mol \quad (3)$$

A feasible methanol synthesis process necessitates a highly efficient catalyst that is both highly active and selective for methanol synthesis and stable over long periods of continuous operation [13]. In a typical methanol synthesis plant, the catalyst lifespan is typically in the range of several years. Supported copper catalysts, which are frequently used in the production of methanol, require an initial period of activation, during which the copper is reduced from cupric oxide to essentially metallic copper under the influence of a diluted hydrogen stream at a high temperature. The initial peak of activity is frequently

followed by a gradual decline in the rate of methanol synthesis. The reactor temperature gradually rises over the course of a catalyst's lifetime to make up for the decline in the catalytic activity [1,14].

Catalysts with high stability and a long lifespan are extremely valuable for developing industrial processes. Nevertheless, catalysts always exhibit deactivation behavior during industrial application. Identifying and investigating the causes of catalyst deactivation, followed by developing more stable catalysts, appears to be crucial. Prior investigation into possible causes of Cu/Zn/Al catalyst deactivation during the production of methanol from syngas has revealed the following: (1) the trace of the contaminant in the feed gas poisoned the catalyst [15,16]; (2) high reaction temperature led to sintering of Cu particles [6]; and (3) carbon deposition [17]. Recently, some new observations for Cu/Zn/Al catalyst deactivation in CO hydrogenation to methanol were made, owing to the advancement of modern characterization techniques. Lunkenbein et al. studied the deactivation behavior of a Cu/Zn/Al catalyst for methanol synthesis over a 148-day time-on-stream (TOS) period. It was proposed that the deactivation was caused primarily by changes in the ZnO moiety, given that ZnO was the most dynamic species and Cu nanoparticles underwent relatively minor modifications [18]. It is worth noting that there are differences between CO hydrogenation and CO_2 hydrogenation for methanol synthesis. The in-situ water formation during CO_2 hydrogenation to methanol may hasten the crystallization of Cu and ZnO components, resulting in the deactivation of Cu/ZnO-based catalysts [19]. The catalyst's dynamic structural changes throughout the deactivation period are still not fully understood, and further research is needed to determine the true causes of deactivation [20].

In this study, the Cu/ZnO/Mn/Nb/Zr/Al_2O_3 catalyst, which was denoted as CZMNZA, was evaluated for extended reaction duration. With the aid of several characterization techniques, the detailed changes in the structural and chemical states of the spent catalysts were investigated, and the stability of the catalyst was comprehensively examined. In addition, the catalyst formulation was expected to enhance CO_2 conversion and methanol selectivity and at the same time slow the rate of deactivation. From a technoeconomic perspective, enhancement in catalytic activity can save capital expenditure (CAPEX) by reducing the number of recycling compressors to reduce the recycling volume.

2. Materials and Methods

2.1. Catalyst Preparation

CZMNZA catalyst was prepared via the wet impregnation method. Firstly, commercially purchased Al_2O_3 support from Merck was heated at 400 °C in flowing Ar for 5 h to eliminate moisture and impurities. The amount of precursor, Cu/ZnO (15 wt.%) with ratio of 70:30 and promoters (0.09 wt.%) with Mn:Nb:Zr ratio of 4:1:1, was calculated based on the prepared total mass of the catalyst. The desired amount of copper (II) nitrate trihydrate ($Cu(NO_3)_2.3H_2O$), zinc nitrate hexahydrate ($Zn(NO_3)_2.6H_2O$), manganese (II) nitrate tetrahydrate ($Mn(NO_3)_2.4H_2O$), ammonium niobate (V), oxalate hydrate ($C_4H_4NNbO_9.xH_2O$), and zirconium (IV) oxynitrate hydrate ($ZrO(NO_3)_2.H_2O$) were dissolved in a required amount of deionized water to produce a 0.5 M aqueous precursor solution. The solution was stirred for one hour to ensure homogeneity. The prepared aqueous precursor solution was then added into a beaker containing Al_2O_3 support in a dropwise manner. The solution's pH was maintained at 7 with the addition of 10% ammonia solution or 10% nitric acid solution. The mixture was filtered and rinsed with deionized water after 24 h of stirring. The paste was dried for 12 h at 120 °C and calcined for 4 h at 350 °C.

2.2. Catalyst Performance Evaluation

The catalyst longevity study was carried out using a stainless steel fixed-bed reactor (Microactivity Reference, PID Eng.Tech) for two, seven, and 14 days. The catalyst powder was reduced in H_2 flow at 243 °C for 6 h and then evaluated for CO_2 hydrogenation reaction at a 300 °C reaction temperature, 31.25 bar reaction pressure, 2160 mL/g.hr GHSV,

and H_2:CO_2 of 10:1. After each reaction period, spent catalyst samples were retrieved and characterized.

2.3. Catalyst Characterization

Textural analysis was performed on a Micromeritics ASAP 2020 analyzer by determining nitrogen adsorption/desorption isotherms at −196 °C. Prior to analysis, the sample was degassed at 350 °C (heating rate 10 °C/min). The Brunauer-Emmett-Teller (BET) specific surface area and pore volume were calculated using the adsorption data. The mean pore diameter of the isotherm desorption branch was calculated using the Barrett-Joyner-Halenda (BJH) model [21]. Morphologies and elemental composition of the samples were observed on the Hitachi SU8020 field emission scanning electron microscope-energy dispersive x-ray (FESEM/EDX). Samples were prepared by dispersing the powdered samples on carbon tape and aluminum tape. Particle size distribution of the spent catalysts was measured using a high-resolution transmission electron microscope (HRTEM). The powdered sample was suspended in isopropanol, followed by ultrasonication for 30 min. The grid was then placed in the sample chamber to analyze the shape of the nanoparticles, the size of metal oxide particles, and the coverage on the support. The N_2O chemisorption technique was used to determine Cu dispersion, surface area, and particle size. The analysis was performed using a Micromeritics Autochem II 2920 instrument. The surface composition of the spent catalyst was determined by x-ray photoelectron spectroscopy (XPS). The XPS spectra were obtained using an XPS Thermo-Fisher K-Alpha instrument. X-ray diffraction (XRD) patterns were carried out on a Shimadzu XRD-7000 by Shimadzu, Japan. The XRD measurements were performed at room temperature using 2θ (Bragg angle) ranging from 10° to 80°, with step size 0.024°/step and 1s/step.

3. Results and Discussion

3.1. Catalyst Performance in Extended Reaction Duration

Table 1 summarizes the results of the stability tests for the CZMNZA catalyst at a reaction duration of 5 h (reference), 2 days, 7 days, and 14 days. Comparing the 2 days reaction results to those of 7 days reaction showed that they remained stable. However, when the reaction duration was prolonged to 14 days, the CO_2 conversion and methanol yield decreased by 5.7% and 7.7%, respectively, whereas methanol selectivity remained nearly stable, as the 1.6% increase can be attributed to experimental uncertainties. Nonetheless, when comparing the methanol selectivity at 14 days to that of 5 h, a significant decrease in methanol selectivity was observed, most likely due to changes in the physicochemical properties of the catalyst. According to the literature, the deactivation rate of a Cu-based catalyst was higher in the first 350 h than it was for longer periods of time [21].

Table 1. Catalytic performance of CZMNZA catalyst in extended reaction durations.

Reaction Duration	CO_2 Conversion, X_{CO2} (%)	MeOH Selectivity, S_{MeOH} (%)	MeOH Yield, Y_{MeOH} (%)
5 h	30.7	66.3	20.3
2 days	27.5	48.8	13.4
7 days	27.5	49.4	13.6
14 days	25.0	50.4	12.6

Reaction conditions: 300 °C, 31.25 bar, 2160 mL/g.hr and H_2: CO_2 at 10:1.

Figure 1a–c shows the time-on-stream (TOS) plots for all extended reactions in terms of CO_2 conversion and MeOH yield. These plots show that the catalytic activity remained relatively stable throughout the tested durations.

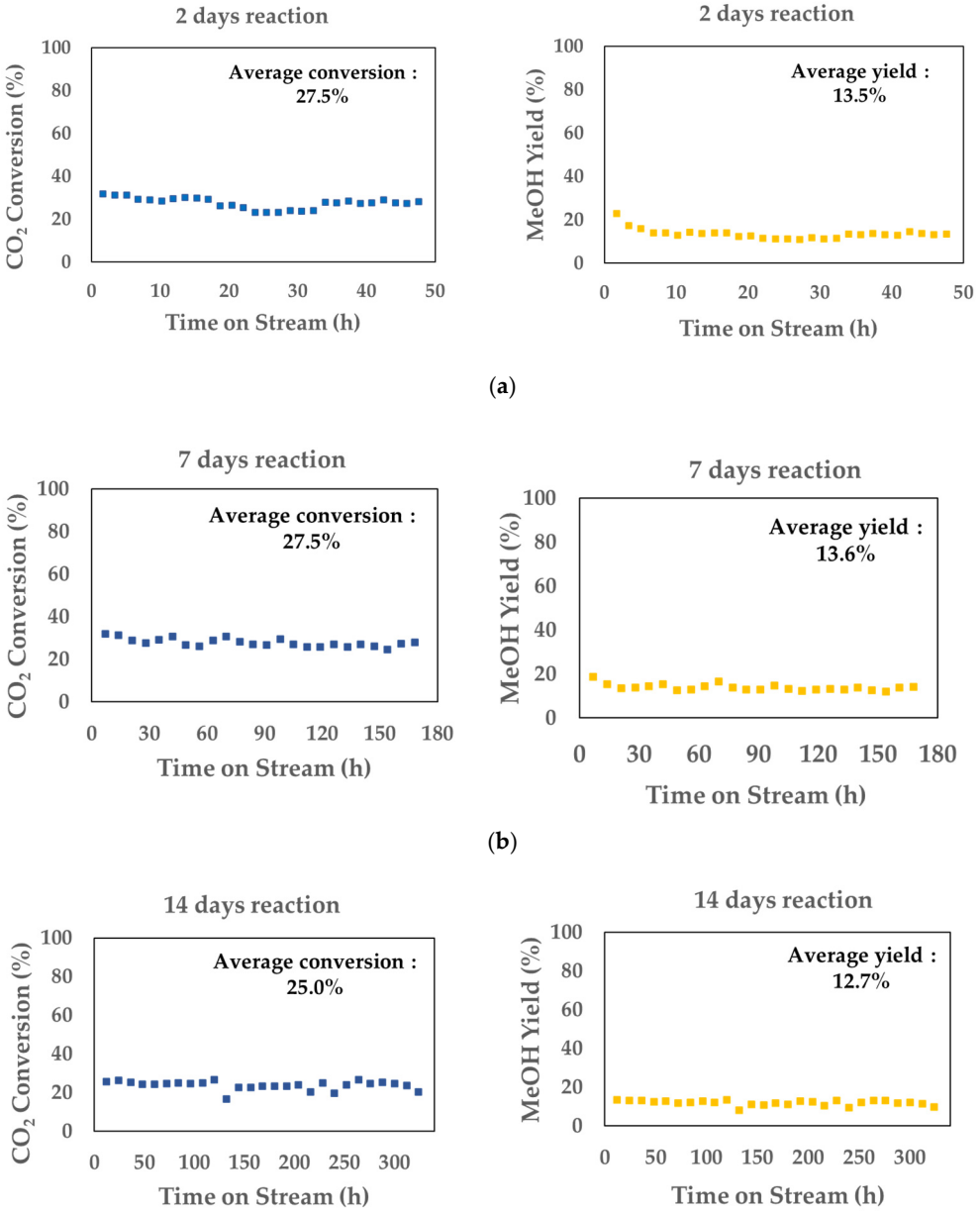

Figure 1. Time-on-stream plots for (**a**) 2 days (**b**) 7 days and (**c**) 14 days reaction.

3.2. Physicochemical Properties of Spent Catalyst

3.2.1. Textural Properties (N_2 Adsorption-Desorption)

Table 2 shows the textural properties of the synthesized catalysts in terms of the BET surface area, pore volume, and pore size. The pore volumes remained the same at 0.2 cm^3/g for all samples. Since N_2 physisorption demonstrated no loss of pore volumes over prolonged exposure to the catalyst, pore clogging did not contribute to the reported catalyst deactivation [22]. The BET surface areas varied between 88.1 and 110.9 m^2/g, and the pore diameters ranged between 7.7 and 8.3 nm. A slight decrease in BET surface areas was observed for all the spent catalysts relative to that of the fresh catalyst sample. On the other hand, the pore size exhibited an increasing trend upon extended reaction duration. This trend suggests that sintering occurred to a lesser extent after the reaction was carried out at 300 °C for a longer duration, possibly due to the presence of water vapor in the

product mixture. Sintering is often observed at high temperatures (>500 °C); however, it can be accelerated by the presence of water vapor [23].

Table 2. Textural properties of catalyst samples.

Samples	BET Surface Area (m^2/g)	Pore Volume (cm^3/g)	Pore Size (nm)
Fresh catalyst	110.9	0.2	7.7
Spent catalyst 5 h	107.8	0.2	8.0
Spent catalyst 2 days	105.0	0.2	8.0
Spent catalyst 7 days	88.1	0.2	8.2
Spent catalyst 14 days	100.4	0.2	8.3

3.2.2. Morphology and Elemental Composition (FESEM/EDX)

The morphologies and elemental mappings of the fresh and spent catalyst samples are depicted in Figure 2a–e. These FESEM images revealed no discernible trend in the morphology of the catalyst after prolonged reaction duration. All the samples have an irregular morphology.

The elemental compositions were determined using EDX analyses on carbon tape and aluminum tape. The results are presented in Tables 3 and 4, respectively. The amount of Cu active metal remained in the range of 16% to 18.1%. The Zr promoter was detected in all samples between 3.4% to 3.7%, while the Mn and Nb promoters were present in some but not all tested samples. The observed variation in the bulk elemental compositions of these elements could be due to sample inhomogeneity during the impregnation process, as suggested by the EDX analysis. Nonetheless, the carbon content of the spent catalysts was higher than that of the fresh catalyst. Although carbon was found on every spent catalyst (Table 4), it did not accumulate significantly enough to clog pores since the pore volumes were constant across all samples. According to the classification of the methanol synthesis reaction as "coke insensitive" [23], carbon formed on active sites can be readily removed by hydrogen or other gasifying agents. This trend suggests that the slight decay in the catalyst performance during prolonged reaction duration may not be entirely due to carbon formation.

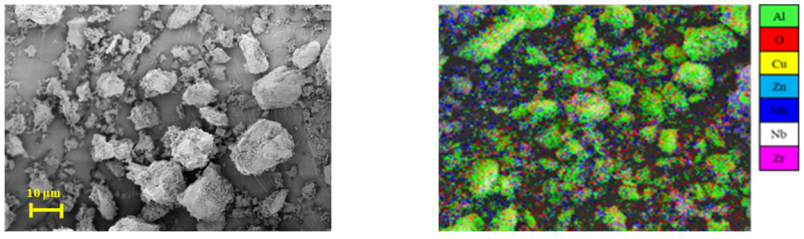

(**a**)

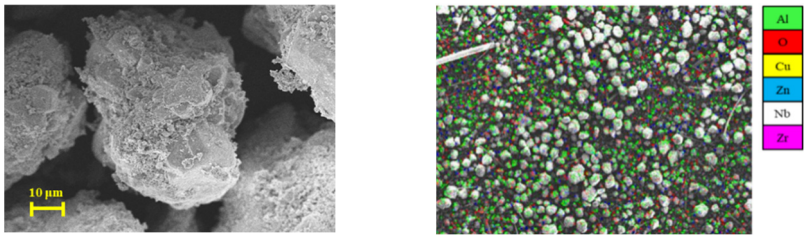

(**b**)

Figure 2. *Cont.*

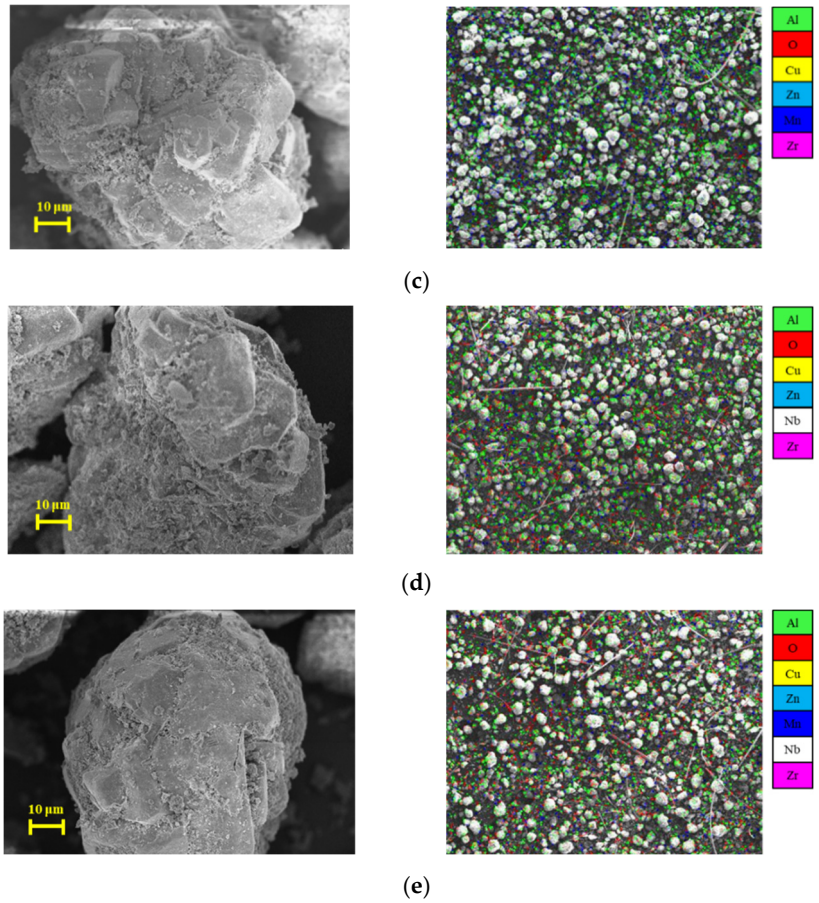

Figure 2. FESEM images and EDX mapping of catalysts for (**a**) fresh (**b**) 5 h (**c**) 2 days (**d**) 7 days and (**e**) 14 days.

Table 3. Elemental compositions of samples using EDX analyses on carbon tape.

Samples	Element (wt.%)						
	Al	**O**	**Cu**	**Zn**	**Mn**	**Nb**	**Zr**
Fresh catalyst	29.87	43.87	16.11	6.33	0.12	0.30	3.40
Spent catalyst 5 h	29.69	43.14	17.34	5.70	-	0.23	3.63
Spent catalyst 2 days	28.98	40.72	18.09	8.48	0.21	-	3.52
Spent catalyst 7 days	30.22	41.20	16.45	8.25	-	0.22	3.66
Spent catalyst 14 days	30.56	41.13	16.43	7.62	0.21	0.40	3.65

Table 4. Elemental compositions of samples using EDX analyses on Al tape.

Samples	Element (wt.%)						
	C	**O**	**Cu**	**Zn**	**Mn**	**Nb**	**Zr**
Fresh catalyst	8.24	76.55	9.70	4.09	0.07	-	1.35
Spent catalyst 5 h	23.73	64.62	7.70	2.83	0.05	0.04	1.03
Spent catalyst 2 days	23.45	62.89	8.83	3.76	0.10	0.07	0.90
Spent catalyst 7 days	20.00	65.25	9.53	4.16	0.01	0.05	1.00
Spent catalyst 14 days	24.91	62.07	8.37	3.67	-	0.05	0.93

3.2.3. Particle Size Distribution (TEM)

Figure 3a–e show TEM images of the catalyst samples. The average particle sizes of the samples are shown in Table 5. It shows a general decreasing trend as reaction duration

increases. After 14 days of reaction, the average particle size was reduced by about 55% compared to that of the fresh catalyst. Particle size reduction was most likely the result of thermal degradation via the redispersion phenomena [20,23]. The redispersion resulted from the formation of volatile metal oxide complexes that attached to the catalyst surface which were subsequently decomposed to smaller crystallites. The particle size distribution of fresh and spent catalysts is shown in Figure 4. Reactions prolonged for up to 14 days showed significantly smaller particle size distribution, which is in agreement with the redispersion mechanism.

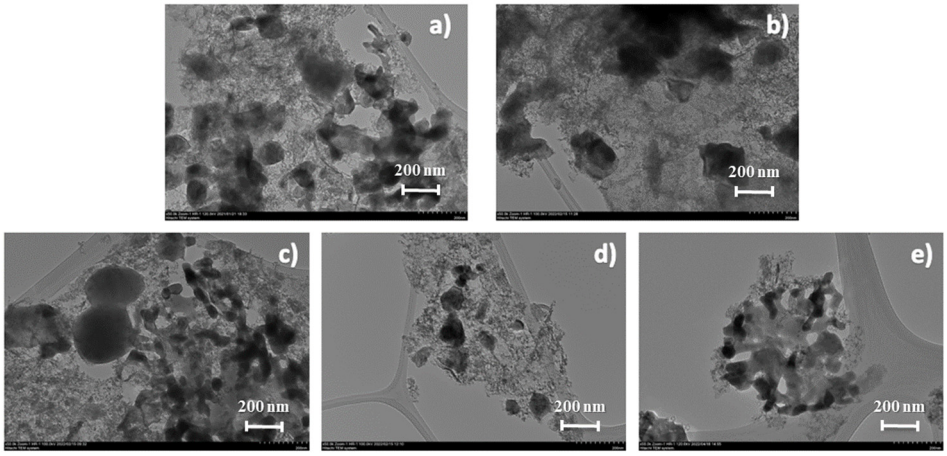

Figure 3. TEM images of (**a**) fresh and spent catalysts after reaction durations of (**b**) 5 h (**c**) 2 days (**d**) 7 days and (**e**) 14 days.

Table 5. Average particle size of catalyst samples.

Samples	Average Particle Size (nm)	Standard Deviation (nm)
Fresh catalyst	20.9	±4.3
Spent catalyst 5 h	22.0	±5.9
Spent catalyst 2 days	11.7	±1.8
Spent catalyst 7 days	10.6	±3.6
Spent catalyst 14 days	9.4	±1.7

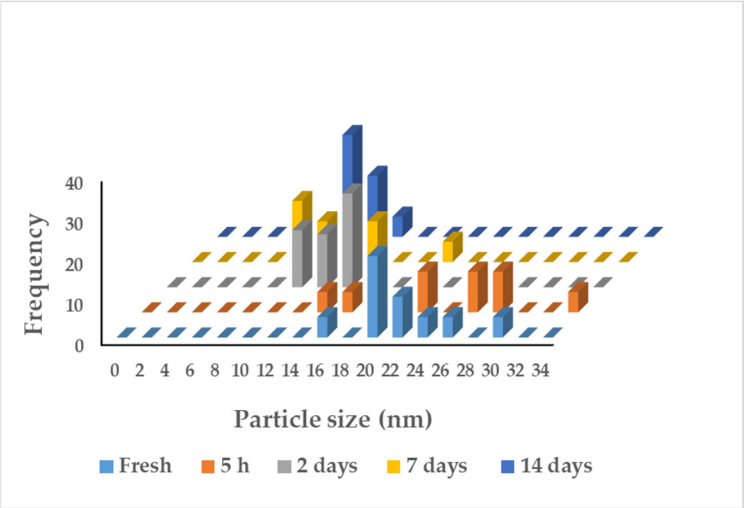

Figure 4. Particle size distribution of fresh and spent catalysts.

3.2.4. Cu Dispersion, Surface Area, and Particle Size (N_2O Chemisorption)

The values of Cu dispersion, Cu surface area, and Cu metal particle size are listed in Table 6. As the reaction duration increased, the Cu dispersion and Cu surface areas

exhibited an upward trend, whereas the Cu particle size showed a reverse trend. These trends agree with the results of TEM analyses which suggest the occurrence of thermal degradation via the redispersion mechanism. The thermal degradation of the catalyst may result in a slight decrease in the catalytic performance over extended reaction durations.

Table 6. Cu dispersion, surface area, and particle size.

Samples	Cu Dispersion (%)	Cu Surface Area (m^2/g)	Cu Particle Size (nm)
Fresh catalyst	10.3	6.2	11.4
Spent catalyst 5 h	9.7	5.8	12.1
Spent catalyst 2 days	14.8	8.9	8.0
Spent catalyst 7 days	13.5	8.1	8.7
Spent catalyst 14 days	16.0	9.6	7.3

According to the literature, the deactivation of Cu-based catalysts during methanol synthesis is primarily due to the aggregation of Cu particles [6,17]. In many cases, sintering, Ostwald ripening, or some other process caused the metal to grow in size at high temperatures. The Cu particle size of the fresh catalyst increased from 11.4 nm to 12.1 nm after 5 h of reaction, while the Cu dispersion decreased from 10.3% to 9.7%. Nevertheless, it is interesting to note that the average size of the Cu particle of the fresh catalyst significantly decreased from 11.4 nm to 8.0 nm after 2 days of reaction, while the Cu surface area significantly increased from 10.3% to 14.8%. This change may have resulted from rebuilding Cu species during the early phase of the reaction [20]. By extending the reaction time from 2 days to 14 days, the size of the Cu particle decreased to 7.3 nm, and the Cu dispersion increased from 14.8% to 16.0%. The dispersion of Cu was not significantly altered. In other words, there was no discernible aggregation of Cu particles throughout the CO_2 hydrogenation reaction phase [20]. Based on these findings, it was suggested that the sintering of Cu particles might not be the primary cause of CZMNZA catalyst deactivation for CO_2 hydrogenation to methanol. This trend in Cu surface area was different from that in BET surface areas obtained from N_2 adsorption-desorption analyses. The BET surface area of the samples decreased after an extended reaction duration, however, the Cu surface area increased. Thus, other factors that affect BET surface area values could be responsible for the variation in the results obtained. Nevertheless, the trend of catalytic activity shows a correlation to Cu surface area in which the catalytic activity remained stable under prolonged reaction durations. This catalyst formulation shows a potential to be used for methanol synthesis via CO_2 hydrogenation in which a similar trend in catalytic activity has been observed to the one reported in the literature [6].

3.2.5. Surface Composition (XPS)

Figure 5a–f show the XPS spectra of Cu 2p, Zn 2p, Mn 2p, Zr 3d, and Nb 3d, respectively. Tables 7 and 8 show the binding energies and atomic compositions, respectively. The surface composition of Cu was detected at 5% on the fresh catalyst and a decreasing trend in Cu:Zn ratio was observed on samples used in longer reaction durations. The observed decrease in Cu:Zn ratios could be due to the enrichment of ZnO particles on the surface of the catalyst, which increased the spacing of the Cu sites. The results from XPS analyses agree with the results of N_2O chemisorption studies, which found an increase in Cu dispersion on spent catalysts as reaction duration increased. The amounts of surface carbon on the spent catalyst samples were higher than those on the fresh catalyst.

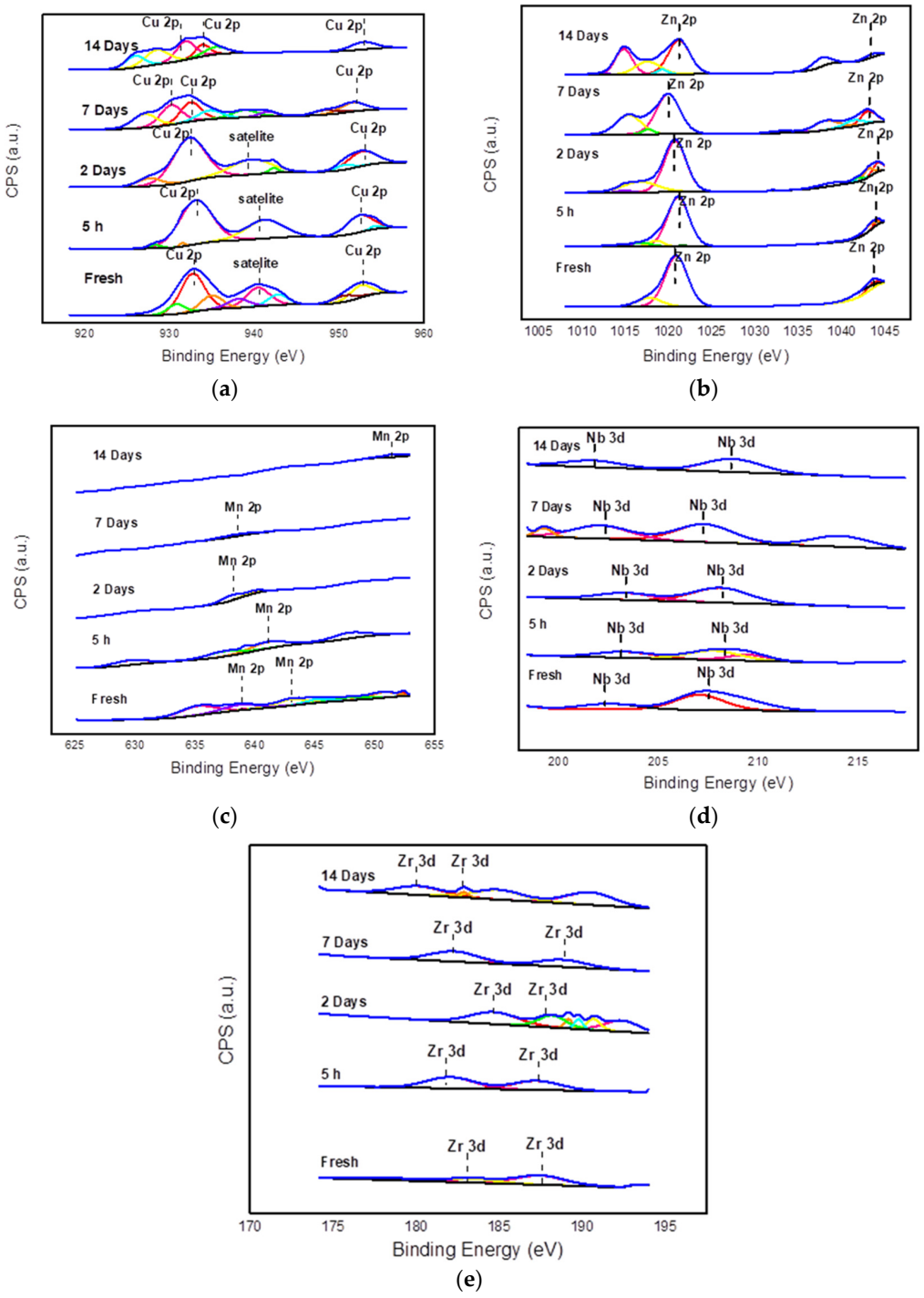

Figure 5. XPS spectra for (**a**) Cu 2p (**b**) Zn 2p (**c**) Mn 2p (**d**) Nb 3d and (**e**) Zr 3d.

However, the C/Al ratios remained constant as reaction durations increased, suggesting that the observed catalyst decay might not be due to carbon formation on the surface of the catalyst. Changes in the oxidation state of Cu have been observed upon the extended duration of the reaction. Cu^{2+} species were found on the fresh catalyst at 932.7 eV, showing that the Cu species for fresh $Cu/ZnO/Al_2O_3$ catalyst primarily existed in the form of CuO [24,25]. It was clearly seen that the shakeup satellite peak at the high binding energy of 941 eV existed, which was another hallmark of the Cu^{2+} compound. This is due to the charge transfer between the 3d orbital of the transition metal and the 2p orbital of the oxygen-containing ligand [26]. There were no significant changes in the peak position of Cu^{2+} in the catalyst after a reaction of 5 h and 2 days, indicating that there

is no difference in the chemical states of copper between the fresh and the spent catalyst which were exposed to reaction gas mixture (CO_2/H_2). The observation in this study is supported by the findings reported by Dai et al. [25]. Nevertheless, the loss of Cu^{2+} species from the surface catalysts can be confirmed by a decrease in shake-up satellite species [26]. Upon extended reaction duration of 7 days and 14 days, mixed oxidation states of Cu, such as 0, +1, and +2 have been detected, suggesting that Cu species can be reduced in the CO_2 hydrogenation environment. The decrease in Cu:Zn ratio is expected in the reductive atmosphere, as reported by Liang et al. [20].

Table 7. Binding energy for each element.

Samples	Binding Energy (eV)				
	Cu $2p_{3/2}$	Zn $2p_{3/2}$	Mn $2p_{3/2}$	Nb $3d_{3/2}$	Zr $3d_{5/2}$
Fresh catalyst	932.7	1020.9	638.9	205.5	183.2
Spent catalyst 5 h	933.1	1021.1	641.1	206.9	182.3
Spent catalyst 2 days	932.3	1020.8	638.2	206.5	185.1
Spent catalyst 7 days	930.2	1020.0	638.4	205.7	182.6
Spent catalyst 14 days	931.9	1021.2	651.5	207.1	183.4

Table 8. Surface atomic composition.

Catalyst	Atomic Composition (%)								Atomic Ratio					
	Al	O	C	Cu	Zn	Mn	Nb	Zr	Cu/Zn	C/Al	Cu/Al	Mn/Al	Nb/Al	Zr/Al
Fresh catalyst	36.6	49.4	0.5	5.0	7.7	1.0	0.1	0.2	0.7	0.01	0.1	0.02	0.003	0.01
Spent catalyst 5 h	23.2	63.8	2.7	5.0	4.5	0.6	0.1	0.1	1.1	0.1	0.2	0.03	0.04	0.04
Spent catalyst 2 days	28.3	57.8	3.0	4.8	5.6	0.1	0.1	0.2	0.9	0.1	0.2	0.04	0.04	0.07
Spent catalyst 7 days	27.7	59.2	4.1	3.0	5.6	0.04	0.2	0.1	0.5	0.1	0.1	0.01	0.07	0.03
Spent catalyst 14 days	27.3	62.0	3.6	2.3	4.9	0.04	0.1	0.2	0.5	0.1	0.1	0.01	0.04	0.07

The binding energies of the Zn $2p_{3/2}$ and Zn $2p_{1/2}$ XPS peaks of the fresh catalyst, which can be observed in Figure 5b are ~1021 eV and ~1044 eV, respectively. These Zn species peaks on the catalyst surface are attributable to Zn^{2+} species in bulk ZnO [27,28]. After 5 h and 14 days of reaction durations, the Zn $2p_{3/2}$ peaks moved toward slightly higher BEs at 1021.1 eV and 1021.2 eV, respectively. This positive chemical shift could be due to the adsorption and heterolysis of H_2 on ZnO. It has been reported that H_2 can be adsorbed by ZnO in the presence of Cu in a reduced Cu/ZnO catalyst, which can lead to heterolysis according to the following expression:

$$\text{H-H} + \text{ZnO} \rightarrow \text{H}^{\delta-}\ \text{Zn-OH}^{\delta+} \quad (4)$$

Thus, the adsorbed hydrogen species at the Zn site ($H^{\delta-}$) may trigger a shift in the Zn 2p core-level peak toward a higher BE position [29]. When the ZnO coverage is increased, the Zn $2p_{3/2}$ peak position decreases, but it remains near the values for Zn^{2+} [30–32]. Some oxygen vacancies may be created inside the oxide layer that covers Cu (111) for significant zinc oxide coverages when hydrogen and oxygen react to form water [33]. The above findings supported the observed increase in the amount of Zn, which resulted in a decreasing trend on the Cu:Zn ratio on the surface of spent catalysts.

The XPS spectra for promoters, Mn 2p, Nb 3d, and Zr 3d are shown in Figure 5c–e. Mn 2p XPS spectra for fresh catalyst were deconvoluted into a few peaks in the binding energy (BE) range of ~638.9 eV to ~651 eV, suggesting the existence of Mn in the catalyst with varied oxidation states. The Mn $2p_{3/2}$ peak can be found to be quite broad, which may be due to the coexistence of various Mn $2p_{3/2}$ levels, Mn^{2+}, Mn^{3+}, and Mn^{4+} species at the interfacial catalyst [34]. The BEs at about 638.9 eV, 642.5 eV, and 651.1 eV can be assigned to

Mn^{2+}, Mn^{3+}, and Mn^{4+}, respectively [35,36]. After a reaction of 2 days and 7 days, a slight shift appears towards lower BE for the Mn^{2+} oxidation state which suggested that Mn^{2+} species can be reduced to metallic Mn. In addition, other Mn species had disappeared after prolonged reaction duration. However, when the reaction was extended up to 14 days, only a single small peak at higher BE was observed which revealed that all Mn species were removed during the extended CO_2 hydrogenation reaction. The atomic composition of Mn also decreased after an extended reaction duration. This observation agrees with the result of EDX analysis on Al tape where no Mn was detected.

The spectrum of the core level Nb 3d is shown in Figure 5d. The appearance of the doublet peaks at $3d_{3/2}$ and $3d_{5/2}$ for the fresh catalyst at 205.5 eV and 204.4 eV, respectively, suggested that the binding energy for NbO/NbO_2 species is in accordance with that of the standard spectra with a slight shift observed [37]. Nevertheless, the binding energy of 205.5 eV was shifted to the right at 206.5 eV–207.1 eV after an extended reaction duration of up to 14 days (except for 7 days), which indicates the presence of Nb_2O_5 [38]. The second peak at 204.4 eV was shifted to the lower binding energy in the range between ~201 eV–203 eV, indicating the existence of metallic Nb [39] and suggesting that during the longer reaction, the metal oxides can be reduced to their metallic form.

The XPS profile for Zr 3d (Figure 5e) revealed two peaks for the fresh, 5 h, and 7 days samples, with the lower binding energy (182 eV–183 eV) indicating the Zr $3d_{5/2}$ orbital and the higher binding energy (185 eV–187 eV) reflected the Zr $3d_{3/2}$ orbital. These values are consistent with those reported in the literature [40]. The 3.0 eV energy difference between these two peaks implies that there are two distinct forms of zirconium ions, with the lower binding energy corresponding to Zr^{4+} (ZrO_2) and the higher binding energy representing Zr^{2+} species [41]. The peaks were shifted to lower and higher binding energies for spent catalysts of 2 days and 14 days, which was caused by hydrogen dissolution. The formation of a Zr-H chemical bond substantially modifies the dependency of core-level changes on the distance between hydrogen and zirconium atoms [42]. In addition, the peak shift to higher binding energy suggests that zirconium's oxidation state has increased. As the reaction prolonged, there may have been a greater proportion of zirconia (ZrO_2) than zirconium oxides ($ZrO_{x,y}$, x,y < 2, higher and lower oxidation states). This could be explained by the fact that zirconium, with a lower oxidation state, completely oxidizes into zirconia with a +4-oxidation state. Whilst it is vice versa for the peak shifting to a lower binding energy [43,44].

3.2.6. Phase Analysis (XRD)

XRD analysis was used to determine the catalyst's phase composition and crystallographic structure. Figure 6 shows the XRD patterns of the CZMNZA catalyst at different stages (fresh, 5 h, 2 days, 7 days, and 14 days). Two significant peaks of gamma aluminum oxide (γ-Al_2O_3) as catalyst support can be identified at 2θ of 45.90° and 67.18° [45] in fresh and all-spent catalysts, which suggested there is no phase change of gamma aluminum oxide pre and post reaction. Tenorite CuO peaks were found in fresh catalyst at 2θ 32.5°, 35.5°, 38.8°, 48.8°, 58.3°, and 61.5° [45]. Under H_2 flow and reaction conditions, the peaks decrease in intensity, with the appearance of Cu (111), Cu (200), and Cu (220) peaks at 43.1°, 50.1°, and 73.7°, respectively, in all spent catalyst. Bulk crystalline CuO in a fresh catalyst is reduced to metallic Cu, an active phase for CO_2 hydrogenation to methanol [46]. Nevertheless, after a reaction duration of 14 days, the peak intensity of metallic Cu was significantly diminished, which may have been caused by a change in the species of Cu [20]. This statement agreed with the change in catalytic performance after 14 days of reaction. On the other hand, zincite and ZnO diffraction peaks of fresh catalyst were observed at 32.5° and 48.8° [45], although the peaks may overlap with CuO peaks [47,48]. The ZnO diffraction peaks did not appear on the spent catalyst samples compared to the fresh catalyst. It was suggested that the metal species agglomeration occurred by blockage of CuO and ZnO surface sites under hydrogenation testing in time on stream, resulting in low catalytic activity [49].

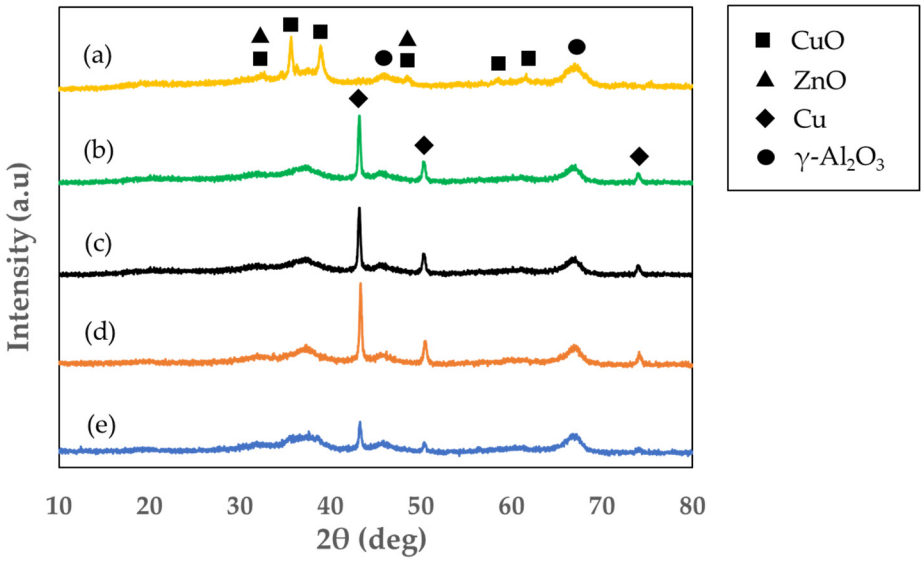

Figure 6. XRD patterns of CZMNZA catalyst of (**a**) fresh (**b**) 5 h (**c**) 2 days (**d**) 7 days and (**e**) 14 days.

4. Conclusions

Cu/ZnO-based catalyst was evaluated for its stability and activity in methanol synthesis via CO_2 hydrogenation. Catalytic activity was stable in a duration of reaction of up to seven days. However, the catalytic activity in terms of CO_2 conversion and methanol yield decreased by about 5.7% and 7.7%, respectively, upon 14 days of reaction. A slight reduction in catalytic activity during prolonged reaction duration has been suggested due to thermal degradation instead of carbon formation. There was no loss of pore volumes over prolonged exposure to the catalyst, and pore-clogging did not contribute to the catalyst deactivation. Surface composition analysis showed changes in metal species after prolonged reaction duration, which was agreed by XRD analysis. N_2O chemisorption and TEM analysis revealed that the redispersion mechanism phenomenon had occurred.

Since catalyst stability and deactivation are crucial in the performance of methanol synthesis reactions, future work should focus on catalyst performance testing using a recycling reactor setup to study the effect of the unconverted feed gases and by-product CO on the catalytic activity. The catalyst aging test with the right standard procedure should also take place to investigate the lifetime of the catalyst which contributed to the downtime of the reactor at an industrial scale.

Author Contributions: Conceptualization, N.A.M.Z.; methodology, N.H.B. and N.A.S.; formal analysis, N.H.B. and N.A.S.; investigation, N.A.M.Z. and N.H.B.; data curation, N.H.B.; writing—original draft preparation, N.H.B.; writing—review and editing, N.A.M.Z. and R.M.R.; visualization, N.H.B. and N.A.S.; supervision, N.A.M.Z. and R.M.R.; project administration, N.A.M.Z. and N.H.B. All authors have read and agreed to the published version of the manuscript.

Funding: This research was funded by the MRA Research Grant (cost center: 015MDO-031) supported by PETRONAS Research Sdn. Bhd. and Universiti Teknologi PETRONAS.

Data Availability Statement: Research data have been provided in the manuscript.

Acknowledgments: The authors acknowledge the support provided by PETRONAS Research Sdn. Bhd. and Universiti Teknologi PETRONAS.

Conflicts of Interest: The authors declare no conflict of interest.

References

1. Chinchen, G.C.; Denny, P.J.; Jennings, J.R.; Spencer, M.S.; Waugh, K.C. Synthesis of methanol: Part 1. Catalysts and kinetics. *Appl. Catal.* **1988**, *36*, 1–65. [CrossRef]
2. Klier, K. Methanol synthesis. In *Advances in Catalysis*; Eley, D.D., Pines, H., Weisz, P.B., Eds.; Academic Press: New York, NY, USA, 1982; pp. 243–313.
3. Waugh, K.C. Methanol Synthesis. *Catal. Today* **1992**, *15*, 51–75. [CrossRef]
4. Wender, I. Reactions of synthesis gas. *Fuel Process. Technol.* **1996**, *48*, 189–297. [CrossRef]
5. Stangeland, K. Catalytic Conversion of CO_2 to Methanol via CO_2 Hydrogenation. PhD Thesis, University of Stavanger, Stavanger, Norway, 2018.
6. Sun, J.T.; Metcalfe, I.S.; Sahibzada, M. Deactivation of $Cu/ZnO/Al_2O_3$ methanol synthesis catalyst by sintering. *Ind. Eng. Chem. Res.* **1999**, *38*, 3868–3872. [CrossRef]
7. Gaikwad, R. Carbon Dioxide to Methanol : Stoichiometric Catalytic Hydrogenation Under High Pressure Conditions. PhD Thesis, Universitat Rovira i Virgili, Tarragona, Spain, 2018.
8. Gesmanee, S.; Koo-Amornpattana, W. Catalytic hydrogenation of CO_2 for methanol production in fixed-bed reactor using Cu-Zn supported on gamma-Al_2O_3. *Energy Procedia* **2017**, *138*, 739–744. [CrossRef]
9. Diez-Ramirez, J.; Dorado, F.; de la Osa, A.R.; Valverde, J.L.; Sanchez, P. Hydrogenation of CO_2 to methanol at atmospheric pressure over Cu/ZnO catalysts: Influence of the calcination, reduction, and metal loading. *Ind. Eng. Chem. Res.* **2017**, *56*, 1979. [CrossRef]
10. Shi, G.; Chen, Q.; Zhang, Q.; Cai, W.; Li, Z.; Zhai, S.; Yu, H.; Tan, F.; Wang, Y. Morphology effect of ZnO support on the performance of Cu toward methanol production from CO_2 hydrogenation. *J. Saudi Chem. Soc.* **2019**, *24*, 42–51. [CrossRef]
11. Yang, B.; Liu, C.; Halder, A.; Teo, E.C.; Martinson, A.B.F.; Seifert, S.; Zapol, P.; Curtiss, L.A.; Vajda, S. Copper cluster size effect in methanol synthesis from CO_2. *J. Phys. Chem. C.* **2017**, *121*, 10406–10412. [CrossRef]
12. Jiang, X.; Nie, X.; Guo, X.; Song, C.; Chen, J.G. Recent advances in carbon dioxide hydrogenation to methanol via heterogeneous catalysis. *Chem. Rev.* **2020**, *120*, 7984–8034. [CrossRef]
13. Saito, M.; Fujitani, T.; Takeuchi, M.; Watanabe, T. Development of copper/zinc oxide-based multicomponent catalysts for methanol synthesis from carbon dioxide and hydrogen. *Appl. Catal. A Gen.* **1996**, *138*, 311–318. [CrossRef]
14. Kung, H.H. Deactivation of methanol synthesis catalysts—A review. *Catal. Today* **1992**, *11*, 443–453. [CrossRef]
15. Radovic, L.R.; Vannice, M.A. Sulfur tolerance of methanol synthesis catalysts: Modelling of catalyst deactivation. *Appl. Catal.* **1987**, *29*, 1–20. [CrossRef]
16. Ma, Y.; Ge, Q.; Li, W.; Xu, H. Study on the sulfur tolerance of catalysts for syngas to methanol. *Catal. Commun.* **2008**, *10*, 6–10. [CrossRef]
17. Zhai, X.; Shamoto, J.; Xie, H.; Tan, Y.; Han, Y.; Tsubaki, N. Study on the deactivation phenomena of Cu-based catalyst for methanol synthesis in slurry phase. *Fuel* **2008**, *87*, 430–434. [CrossRef]
18. Lunkenbein, T.; Girgsdies, S.; Kandemir, T.; Thomas, N.; Behrens, M.; Schlögl, R. Bridging the time gap: A copper/zinc oxide/aluminum oxide catalyst for methanol synthesis studied under industrially relevant conditions and time scales. *Angew. Chem. Int. Ed.* **2016**, *55*, 12708–12712. [CrossRef]
19. Wu, J.; Saito, M.; Takeuchi, M.; Watanabe, T. The stability of Cu/ZnO-based catalysts in methanol synthesis from a CO_2-rich feed and from a CO-rich feed. *Appl. Catal. A Gen.* **2001**, *218*, 235–240. [CrossRef]
20. Liang, B.; Ma, J.; Su, X.; Yang, C.; Duan, H.; Zhou, H.; Deng, S.; Li, L.; Huang, Y. Investigation on deactivation of $Cu/ZnO/Al_2O_3$ catalyst for CO_2 hydrogenation to methanol. *Ind. Eng. Chem. Res.* **2019**, *58*, 9030–9037. [CrossRef]
21. Chen, C.S.; Cheng, W.H.; Lin, S.S. Study of reverse water gas shift reaction by TPD, TPR and CO_2 hydrogenation over potassium-promoted Cu/SiO_2 catalyst. *Appl. Catal. A Gen.* **2003**, *238*, 55–67. [CrossRef]
22. Prieto, G.; Meeldijk, J.D.; De Jong, K.P.; De Jongh, P.E. Interplay between pore size and nanoparticle spatial distribution : Consequences for the stability of $CuZn/SiO_2$ methanol synthesis catalysts. *J. Catal.* **2013**, *303*, 31–40. [CrossRef]
23. Argyle, M.D.; Bartholomew, C.H. Heterogeneous catalyst deactivation and regeneration: A review. *Catalysts* **2015**, *5*, 145–269. [CrossRef]
24. Zhu, Y.; Kong, X.; Zhu, S.; Dong, F.; Zheng, H.; Zhu, Y.; Li, Y.W. Construction of $Cu/ZrO_2/Al_2O_3$ composites for ethanol synthesis: Synergies of ternary sites for cascade reaction. *Appl. Catal. B Environ.* **2015**, *166–167*, 551–559. [CrossRef]
25. Dai, W.-L.; Sun, Q.; Deng, J.-F.; Wu, D.; Sun, Y.-H. XPS studies of $Cu/ZnO/Al_2O_3$ ultra-fine catalysts derived by a novel gel oxalate co-precipitation for methanol synthesis by CO_2+H_2. *Appl. Surf. Sci* **2001**, *177*, 172–179. [CrossRef]
26. Sharma, S.K.; Khan, T.S.; Singha, R.K.; Paul, B.; Poddar, M.K.; Sasaki, T.; Bordoloi, A.; Samanta, C.; Gupta, S.; Bal, R. Design of highly stable MgO promoted Cu/ZnO catalyst for clean methanol production through selective hydrogenation of CO_2. *Appl. Catal. A Gen.* **2021**, *623*, 118239. [CrossRef]
27. Qi, T.; Li, W.; Li, H.; Ji, K.; Chen, S.; Zhang, Y. Yttria-doped Cu/ZnO catalyst with excellent performance for CO_2 hydrogenation to methanol. *Mol. Catal.* **2021**, *509*, 111641. [CrossRef]
28. Mousavi-Kamazani, M. Facile sonochemical-assisted synthesis of $Cu/ZnO/Al_2O_3$ nanocomposites under vacuum: Optical and photocatalytic studies. *Ultrason. Sonochem.* **2019**, *58*, 104636. [CrossRef] [PubMed]
29. Kokes, R.J.; Dent, A.L. Butene isomerization over zinc oxide. *J. Phys. Chem.* **1971**, *75*, 487–491. [CrossRef]

30. Nakamura, J.; Nakamura, I.; Uchijima, T.; Kanai, Y.; Watanabe, T.; Saito, M.; Fujitani, T. A surface science investigation of methanol synthesis over a Zn-deposited polycrystalline Cu surface. *J. Catal.* **1996**, *160*, 65–75. [CrossRef]
31. Campbell, C.T.; Daube, K.A.; White, J.M. Cu/ZnO(0001) and ZnOx/Cu(111): Model catalysts for methanol synthesis. *Surf. Sci.* **1987**, *182*, 458–476. [CrossRef]
32. Vohs, J.M.; Barteau, M.A. Spectroscopic characterization of surface formates produced via reaction of HCOOH and $HCOOCH_3$ on the (0001) surface of zinc oxide. *Surf. Sci.* **1988**, *197*, 109–122. [CrossRef]
33. Senanayake, S.D.; Ramirez, P.J.; Waluyo, I.; Kundu, S.; Mudiyanselage, K.; Liu, Z.; Liu, Z.; Axnanda, S.; Stacchiola, D.J.; Evans, J.; et al. Hydrogenation of CO_2 to methanol on CeOx/Cu(111) and ZnO/Cu(111) catalysts: Role of the metal–oxide interface and importance of Ce^{3+} sites. *J. Phys. Chem. C* **2016**, *120*, 1778–1784. [CrossRef]
34. Wang, Z.; Shen, G.; Li, J.; Liu, H.; Wang, Q.; Chen, Y. Catalytic removal of benzene over CeO_2-MnOx composite oxides prepared by hydrothermal method. *Appl. Catal. B Environ.* **2013**, *138–139*, 253–259. [CrossRef]
35. Huang, Z.; Zhou, W.; Ouyang, C.; Wu, J.; Zhang, F.; Huang, J.; Gao, Y.; Chu, J. High performance of Mn-Co-Ni-O spinel nanofilms sputtered from acetate precursors. *Sci. Rep.* **2015**, *5*, 2–9. [CrossRef] [PubMed]
36. Jampaiah, D.; Tur, K.M.; Venkataswamy, P.; Ippolito, S.J.; Sabri, Y.M.; Tardio, J.; Bhargava, S.K.; Reddy, B.M. Catalytic oxidation and adsorption of elemental mercury over nanostructured CeO_2–MnOx catalyst. *RSC Adv.* **2015**, *5*, 30331–30341. [CrossRef]
37. Milošev, I.; Kosec, T.; Strehblow, H.H. XPS and EIS study of the passive film formed on orthopaedic Ti–6Al–7Nb alloy in Hank's physiological solution. *Electrochim. Acta* **2008**, *53*, 3547–3558. [CrossRef]
38. Li, M.; Jiao, L.; Nawaz, M.A.; Cheng, L.; Meng, C.; Yang, T.; Tariq, M.; Liu, D. A one-step synthesis method of durene directly from syngas using integrated catalyst of Cu/ZnO/Al_2O_3 and Co-Nb/HZSM-5. *Chem. Eng. Sci.* **2019**, *200*, 103–112. [CrossRef]
39. Wong, K.C.; Wong, P.C.; Li, Y.S.; Mitchell, K.A.R. Chemical properties of a Nb/Zr interface studied by XPS. *Surf. Rev. Lett.* **1997**, *4*, 33–37. [CrossRef]
40. Marakatti, V.S.; Marappa, S.; Gaigneaux, E.M. Sulfated zirconia: An efficient catalyst for the Friedel-Crafts monoalkylation of resorcinol with methyl tertiary butyl ether to 4-tertiary butylresorcinol. *New J. Chem.* **2019**, *43*, 7733–7742. [CrossRef]
41. Din, I.U.; Shaharun, M.S.; Subbarao, D.; Naeem, A.; Hussain, F. Influence of niobium on carbon nanofibres based Cu/ZrO_2 catalysts for liquid phase hydrogenation of CO_2 to methanol. *Catal. Today* **2016**, *259*, 303–311. [CrossRef]
42. Svyatkin, L.A.; Lopatina, O.V.; Chernov, I.P.; Koroteev, Y.M. Core electron level shifts in zirconium induced by vacancy, helium and hydrogen. *Comput. Mater. Sci.* **2018**, *153*, 176–182. [CrossRef]
43. Sun, Y.-M.; Lozano, J.; Ho, H.; Park, H.J.; Veldman, S.; White, J.M. Interfacial silicon oxide formation during synthesis of ZrO_2 on Si(100). *Appl. Surf. Sci.* **2000**, *161*, 115–122. [CrossRef]
44. Zhang, N.L.; Song, Z.T.; Shen, Q.W.; Wu, Y.J.; Liu, Q.B.; Lin, C.L. High frequency capacitance–voltage characterization of $Al_2O_3/ZrO_2/Al_2O_3$ in fully depleted silicon-on-insulator metal–oxide–semiconductor capacitors. *Appl. Phys. Lett.* **2003**, *83*, 5238–5240. [CrossRef]
45. Halim, N.S.A. Synthesis, Characterization and Performance of Copper-Zinc Oxide with Mixed Promoter Catalyst for CO_2 Hydrogenation to Methanol. Master's Thesis, Universiti Teknologi Petronas, Perak, Malaysia, 2019.
46. Natesakhawat, S.; Lekse, J.W.; Baltrus, J.P.; Ohodnicki, P.R., Jr.; Howard, B.H.; Deng, X.; Matranga, C. Active sites and structure-activity relationships of copper-based catalysts for carbon dioxide hydrogenation to methanol. *ACS Catal.* **2012**, *2*, 1667–1676. [CrossRef]
47. Huang, C.; Chen, S.; Fei, X.; Liu, D.; Zhang, Y. Catalytic hydrogenation of CO_2 to methanol: Study of synergistic effect on adsorption properties of CO_2 and H_2 in CuO/ZnO/ZrO_2 system. *Catalysts* **2015**, *5*, 1846–1861. [CrossRef]
48. Li, Z.; Yan, S.; Fan, H. Enhancement of stability and activity of Cu/ZnO/Al_2O_3 catalysts by microwave irradiation for liquid phase methanol synthesis. *Fuel* **2013**, *106*, 178–186. [CrossRef]
49. Kamsuwan, T.; Krutpijit, C.; Praserthdam, S.; Phatanasri, S.; Jongsomjit, B.; Praserthdam, P. Comparative study on the effect of different copper loading on catalytic behaviors and activity of Cu/ ZnO/Al_2O_3 catalysts toward CO and CO_2 hydrogenation. *Heliyon* **2021**, *7*, e07682. [CrossRef] [PubMed]